Microporous and Mesoporous Materials 305 (2020) 110287

Contents lists available at ScienceDirect

Microporous and Mesoporous Materials

journal homepage: http://www.elsevier.com/locate/micromeso

# Solid-state NMR study of adsorbed water molecules in covalent organic framework materials

Jiaqi Ma [a,1], Xiao-Bin Fu [b,1], Yuquan Li [a], Tian Xia [a], Likun Pan [a], Ye-Feng Yao [a,*]

[a] Physics Department and Shanghai Key Laboratory of Magnetic Resonance, School of Physics and Electronic Science, East China Normal University, Shanghai, 200062, China

[b] Key Laboratory of Interfacial Physics and Technology, Shanghai Institute of Applied Physics, Chinese Academy of Sciences, Shanghai, 201800, China

ARTICLE INFO

*Keywords:*
Water adsorption
Covalent organic framework materials
Solid state NMR
Water molecule redistribution
Porous material

ABSTRACT

This study investigates the locations and interactions of adsorbed water molecules within a porous COF material, TpPa-1. The TpPa-1 samples include the as-synthesized powder samples and the samples first subjected to compression at high pressure and then ground into a powder form. The investigation applies a variety of advanced solid-state NMR techniques. The results indicate that the adsorbed water molecules in the as-synthesized and compressed samples can exist in different locations and bonding states. Here, the adsorbed water molecules in the as-synthesized samples are found to be mainly located in the pore spaces and interact only loosely with the chemical groups of the material. In contrast, a proportion of the water molecules in the compressed samples enter into the interstices between the layers and interact with the amino groups and the carbonyl groups of the material. The relocation of the water molecules in the compressed samples provides a plausible explanation for the molecular origin of the water adsorption capability of TpPa-1. In addition, the revealed weak interactions between the water molecules and the chemical groups of TpPa-1 are correlated with the molecular origin of the high water permeance.

## 1. Introduction

Covalent organic framework (COF) materials are characterized by ordered pore structures with nanoscale diameters [1]. These characteristic pore structures generate very large surface areas that make COF materials highly promising for applications involving ion separation [2–4], adsorption [5–7], and catalysis [8,9]. In addition, COF materials with varying functionality have been developed by introducing functional groups on the pore surfaces, and these materials have demonstrated greater efficiency and specificity for adsorbing targeted molecules than conventional COFs [10–12]. However, the pore surfaces of COFs often absorb non-targeted molecules, like many other porous materials [12], and this can lead to unpredictable changes in the surface properties [13]. For example, a recent work by Wang et al. [14] presented COF films exhibiting rapid color change on their surfaces owing to the adsorption of a wide variety of small organic molecules.

Past research suggests that water molecules are probably the most common unintended adsorbate of COF materials [15]. This is because many COFs contain hydrophilic chemical structures such as amino groups, hydroxyl groups, and carbonyl groups [1,16,17], which are prone to form hydrogen bonds with water molecules, and thereby facilitate their absorption. For example, Biswal et al. [18] applied surface engineering to develop a class of COFs with high water adsorption capacities. Interestingly, these results also demonstrated that the water adsorption capacities of the COFs materials were clearly dependent on the pressure. The observed pressure-induced water adsorption capacity was tentatively attributed to hydrogen bonding between the water molecules and the chemical structures of the COFs. In addition, we note that the water adsorption capacity of COF materials is strongly related to the transport of water molecules through the pore spaces (i.e., water permeance). As such, the mechanisms affecting the water adsorption capacity of COF materials are also operative with respect to water permeance. For example, Zhou et al. [4] investigated the molecular processes related to water transport in COF materials based on theoretical calculations. The results indicated that both hydrogen bonding and the interactions between oxygen and nitrogen atoms on the pore walls and water molecules affected the transport behavior of water molecules through a multilayered COF material. However, despite the wide range

* Corresponding author.
*E-mail address:* yfyao@phy.ecnu.edu.cn (Y.-F. Yao).
[1] J. M. and X.-B. F. contribute equally to this work.

https://doi.org/10.1016/j.micromeso.2020.110287
Received 31 January 2020; Received in revised form 21 April 2020; Accepted 22 April 2020
Available online 5 May 2020

of research focused on water adsorption and ion separation in COFs, some fundamental questions related to the effect of water molecule adsorption and transport in COFs on the water adsorption capacity remain unclear. In particular, it remains unclear how pressure affects the location of adsorbed water molecules in COF materials and how it affects the interactions between water molecules and the chemical structures of COFs.

This is addressed in the present study by investigating the state of water molecules absorbed on the surface of a standard COF material synthesized from the Schiff base reaction of 2,4,6-trihydroxybenzene-1,3,5-tricarbaldehyde (Tp) with *para*-phenylenediamine (Pa-1) [16], which is commonly denoted as TpPa-1. The TpPa-1 samples include as-synthesized powder samples and powder samples first subjected to compression at high pressure and then ground into a powder form. The investigation applies various advanced solid-state nuclear magnetic resonance (NMR) techniques, such as two-dimensional (2D) proton ($^1$H) double quantum-single quantum (DQ-SQ) correlation spectroscopy, $^{13}$C cross-polarization/total sideband suppression (CP/TOSS) and CP/magic-angle spinning (CP/MAS) techniques, and 2D $^1$H–$^{13}$C MAS heteronuclear correlation (HETCOR) spectroscopy, to study the interactions between water molecules and the different chemical groups on the surfaces of the materials. The effect of compression on the water adsorption states of the sample is evaluated by comparing the results obtained for the as-synthesized samples and the compressed samples. The results indicate that the water molecules in the as-synthesized samples interact only loosely with the chemical structures on the material surface, whereas a proportion of the water molecules in the compressed samples enter into the interstices between the TpPa-1 layers and interact with the amino groups and the carbonyl groups. The molecular origin of the water adsorption capability of the material is then discussed in terms of the relocation of the water molecules within the compressed samples. The discovered weak interactions between the water molecules and the chemical groups of TpPa-1 are correlated to the molecular origin of the rapid water molecule transport of the material, and thus its high water permeance.

## 2. Experimental

### 2.1. Materials

Tp (95%) was purchased from Shanghai Bidepharm Tech Co. Ltd, and 1,3,5-trimethylbenzene (98%), 1,4-dioxane (≥99.5%), and deuterium oxide (99.9% D atoms) were purchased from Aladdin Shanghai Co. Ltd. N, *N*-dimethylformamide (DMF; 99.8%), ethanol (≥99.5%), and Pa-1 (≥99%) were purchased from Sigma Aldrich.

### 2.2. Synthesis of TpPa-1

The TpPa-1 synthesis process was conducted according to the work of Kandambeth et al. [16] with slight modifications. Here, Tp (126 mg, 0.6 mmol) and Pa-1 (96 mg, 0.9 mmol) were thoroughly mixed in a solvent composed of 3 M acetic acid (0.5 mL) and trimethylbenzene/-dioxane (3 mL; 1:1 v/v), and the mixture was added to a Schlenk flask for conducting the Schiff reaction. The Schlenk flask was then filled with nitrogen gas, sealed, and held at 90 °C for 24 h. The resulting dark red powder was collected after solvent exchange with DMF and ethanol. Then the powder was put into a vacuum oven for 24 h to get rid of the residual solvents (see Fig. S1). Afterwards, in order to uptake the water, the sample was put into an oven having a constant humidity of 80% for 48 h. The humidity in the oven was controlled by putting a beaker of water inside and setting the temperature of oven to 298 K. The hygrometer showed that the relative humidity in the oven was 80% after the evaporation of the water in the beaker reached equilibrium. After this procedure, the water content in the sample was 22.3% (see Fig. S2 in Supplementary Information). Powder samples (100 mg) were exclusively employed for all testing.

### 2.3. Preparation of compressed TpPa-1

Compressed samples were obtained by pressing 50 mg of TpPa-1 powder into sheets with a 15 mm diameter and ~120 nm thickness using a uniaxial hydraulic press operated at a pressure of 10 MPa. The compressed samples show the colors different to the original powder sample (see Fig. S3 in Supplementary Information). The procedure was repeated to obtain a total of 2 sheets, which were then ground to obtain compressed TpPa-1 powder samples. After the compress process, the water content in the sample was 22.6% (see Fig. S2 in Supplementary Information).

### 2.4. Sample characterization

The $^1$H and $^{13}$C solid-state NMR experiments were performed on a Bruker AVANCE III 600 WB spectrometer operating at 600.44 MHz and 150.98 MHz for $^1$H and $^{13}$C respectively. A 4 mm triple resonance MAS probe was used for the experiments. In $^1$H–$^{13}$C cross polarization under magic angle spinning (CP/MAS) NMR experiments, the cross polarization time was set to 1 ms and the spinning rate was set to 5 kHz. $^{13}$C cross-polarization/total sideband suppression (CP/TOSS) was applied in order to suppress the spin side band. In 2D $^1$H–$^{13}$C HETCOR experiments, FSLG decoupling was applied during the $^1$H dimension and the RF field was set to 100 kHz. In 2D $^1$H–$^{13}$C HETCOR experiments, the CP contact time was set to 200 μs and the MAS spinning rate was set to 10 kHz. In the $^1$H–$^1$H double quantum (DQ)-single quantum (SQ) correlation experiments, the back-to-back (BABA) recoupling sequence was used for the excitation and reconversion of DQ coherences. The used recoupling sequence consists of a two-rotor-period: $(\pi/2)_x$-τ-$(\pi/2)_x$-$(\pi/2)_y$-τ-$(\pi/2)_y$-$(\pi/2)_x$-τ-$(\pi/2)_x$-$(\pi/2)_y$-τ-$(\pi/2)_y$ [19], where τ is $t_R/2$ minus the pulse durations ($t_R$: rotor period). A "z-filter" was used before the final 90° reading pulse, with the duration equal to two rotor periods. In the 2D experiments, signals in the F1 dimension were restored by the TPPI [20] scheme of increasing the phase of the excitation pulses by 45°. In the 2D $^1$H–$^1$H DQ-SQ NMR experiments, a 3.2 mm double resonance MAS probe was used and the MAS spinning rate was set to 20 kHz. The $^1$H pulse width was 2.5 μs and the recycle delay was 4 s. The $^1$H and $^{13}$C chemical shifts were calibrated using adamantane ($\delta = 1.85$ ppm [21] for $^1$H and $\delta = 38.5$ ppm for $^{13}$C respectively).

X-ray Diffraction Measurements were performed on Rigaku, Ultima IV using Cu-Kα (1.5406 Å) radiation (30 kV, 25 mA). All samples were mounted on the same sample holder and scanned from $2\theta = 5°$–$35°$ at a speed of 5°/min. The experimental temperature is room temperature.

The specific surface area and pore size distribution were determined by the nitrogen adsorption-desorption measurements (ASAP 2020 physisorption analyzer) based on the Brunauer-Emmett-Teller (BET) multipoint method and Quenched-Solid Density Functional Theory (QSDFT) calculations. For the as-synthesized TpPa-1, total pore volume = 0.208 cc/g with an average pore diameter of 10.07 Å and BET surface area is 203.615 $m^2$/g. For the compressed TpPa-1, total pore volume = 0.357 cc/g with an average pore diameter of 10.51 Å and BET surface area is 310.159 $m^2$/g. The increased BET surface area in the compressed sample can be attributed to the interstices between the grains which may become some pore-like structures after compression and in turn have the contribution in the nitrogen adsorption-desorption measurements. The $N_2$ sorption isotherm curves and the porosity plots of the samples are referred to Fig. S4 in Supporting Information.

## 3. Results and discussion

As presented elsewhere [16], TpPa-1 forms 2D nanosheets with uniformly ordered sub-5 nm pores penetrating through their 2D planes. The individual sheets are packed together via van der Waals forces to form a laminar structure. Fig. 1a presents a schematic illustrating the packing structure and chemical structure of TpPa-1. Fig. 1b presents wide-angle XRD (WAXD) patterns for representative as-synthesized and

compressed powder samples. The diffraction peaks at $2\theta = 4.51°$, 7.83°, 11.97°, and 26.19° can be attributed to (100), (210), {(310), (320)}, and {(001), (101)} planes, respectively [16]. The very similar diffraction peaks observed for the as-synthesized and compressed samples in Fig. 1b indicate that the compression process induces no significant changes in the crystal structure of TpPa-1. Fig. 1c presents the $^{13}C$ CP/MAS NMR spectra of the as-synthesized and compressed samples. The $^{13}C$ spectra of the samples plotted in the full range (-15 - 285 ppm) can be found in Fig. S5 in Supplementary Information. The peaks in the range between 180 and 188 ppm are assigned to carbonyl groups (C1), while the peaks at 146.0 ppm, 135.7 ppm, 120.9 ppm, 114.8 ppm, and 106.8 ppm are assigned to C2, C3, C4, C5, and C6, respectively, according to the schematic presented at the bottom of Fig. 1a [16]. The very similar $^{13}C$ CP/MAS NMR spectra obtained for the as-synthesized and compressed samples indicate that the chemical structures of TpPa-1 remain consistent after applying the compression process.

Fig. 2a presents the solid state $^{1}H$ MAS NMR spectra of the as-synthesized and compressed samples, which were acquired using single pulse excitation. The observed peaks in the two spectra are quite similar and pertain to the components of the TpPa-1 molecule illustrated schematically on the left side of Fig. 2a. The peak centered at ~2.0 ppm ($H_a$) is assigned to the protons of the aromatic rings. The peak centered at ~2.5 ppm ($H_b$) is assigned to the protons of the vinyl groups. The strong peak centered at ~4.5 ppm ($H_c$) is assigned to water molecules (see Fig. S6 in Supplementary Information). Finally, the very wide signal centered at ~8.0 ppm is assigned to the protons of the amino groups. The relatively large chemical shifts and chemical shift distribution observed in the $^{1}H$ MAS NMR spectra indicate that the amino groups and the neighboring carbonyl groups are likely to form strong intramolecular hydrogen bonds [22–24] and the mutual shielding created by the aromatic rings [25,26].

Fig. 2b presents the 2D $^{1}H$ homonuclear DQ-SQ correlation spectrum of the as-synthesized TaPa-1 powder sample. Here, the cross peaks in a 2D $^{1}H$ DQ-SQ spectrum indicate a close through-space contact between two $^{1}H$ spins, and DQ peaks between identical $^{1}H$ spins (i.e., having the same chemical shift) appear on the diagonal of the 2D spectrum. This is the case in the spectrum in Fig. 2b, where the DQ peaks are centered at 2.0 ppm on the horizontal F2 axis and 4.0 ppm on the vertical F1 axis for the protons of the aromatic rings ($H_a$ - $H_a$ and $H_b$ - $H_b$), and at 8.0 ppm (F2) and 16.0 ppm (F1) for the protons of the amino groups ($H_d$ - $H_d$). Interestingly, no cross peaks from the water molecules are observable in

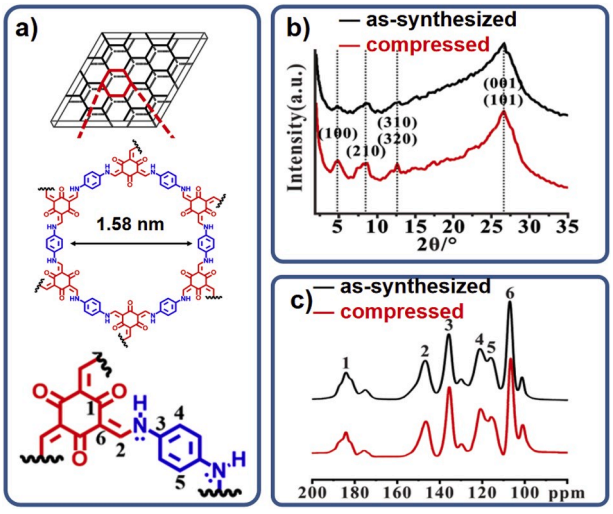


**Fig. 1.** a) Schematic illustrating the 2D laminar packing structure and chemical structure of TpPa-1. b) WAXD patterns of representative as-synthesized and compressed TpPa-1 powder samples. c) Solid-state $^{13}C$ CP/MAS NMR spectra of representative as-synthesized and compressed TpPa-1 samples. All experiments were conducted at room temperature (293 K).

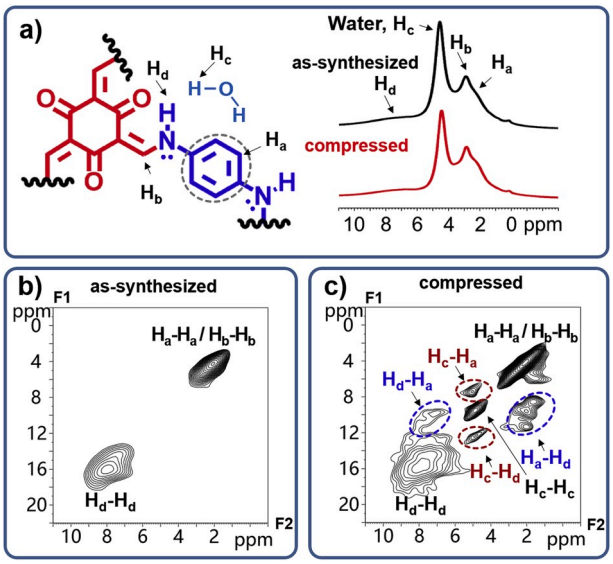


**Fig. 2.** a) $^{1}H$ MAS solid state NMR spectra of representative as-synthesized and compressed TpPa-1 samples. $^{1}H$–$^{1}H$ DQ-SQ NMR spectra of b) an as-synthesized TpPa-1 sample and c) a compressed TpPa-1 sample. All experiments were conducted at 293 K.

the spectrum, indicating that the water molecules in the as-synthesized sample only loosely interact with the chemical groups of TaPa-1. For the origin of the correlation peak ($H_a$ - $H_a$), according to the chemical structure of TpPa-1, it can be attributed to the dipolar interaction of the protons of an individual aromatic ring. For the correlation peak ($H_b$ - $H_b$), it's origin seem to be different. From the chemical structure of TpPa-1, the vinyl group has only one proton that is not possible to have the dipolar interaction by itself. Moreover, there are six bonds between the nearest two vinyl groups in an individual TpPa-1 molecular plane, which is too far to have a strong enough dipolar interaction to give rise to the correlation peak in the spectrum. Therefore, the origin of the correlation peak ($H_b$ - $H_b$) most likely can be attributed to the dipolar interaction between the vinyl groups from the two neighbored layers. Similarly, the origin of the correlation peak ($H_d$ - $H_d$) can also be attributed to the dipolar interaction between the amino groups from the two neighbored layers.

Fig. 2c presents the DQ-SQ spectrum of the compressed TaPa-1 powder sample, which was acquired under the same experimental conditions as that given in Fig. 2b. In contrast to Fig. 2b, many DQ peaks are observed in the spectrum. Here, the diagonal signals at (F2, F1) values of (2.0 ppm, 4.0 ppm), (2.5 ppm, 5.0 ppm), (4.7 ppm, 9.4 ppm), and (7.7 ppm, 15.4 ppm) can be assigned to the correlation peaks derived from the protons of the aromatic rings ($H_a$ - $H_a$), the vinyl groups ($H_b$ - $H_b$), the water molecules ($H_c$ - $H_c$), and the amino groups ($H_d$ - $H_d$), respectively. In addition, correlation peaks are also observed between the protons of the water molecules and the aromatic rings at (4.7 ppm, 6.7 ppm) ($H_c$ - $H_a$), between those of the amino groups and the aromatic rings at (7.7 ppm, 9.7 ppm) ($H_d$ - $H_a$) and (2.0 ppm, 9.7 ppm) ($H_a$ - $H_d$), and between those of the water molecules and the amino groups (4.7 ppm, 12.4 ppm) ($H_c$ - $H_d$). The presence of these correlation peaks indicates that the water molecules in the compressed TpPa-1 powder sample are interacting with the chemical groups of TpPa-1.

Further insight into how the water molecules interact with the chemical groups of TaPa-1 can be obtained from the results of 2D $^{1}H$–$^{13}C$ HETCOR experiments presented in Fig. 3a and b for the as-synthesized and compressed samples, respectively. In these spectra, the F1 axis corresponds to the $^{1}H$ chemical shift range of −4 to 10 ppm, which is vertical in the figure, and the F2 axis corresponds to the $^{13}C$ chemical shift range of 90–190 ppm, which is horizontal in the figure. Contours in the spectrum result from individual $^{1}H$–$^{13}C$ spin pairs correlated by the

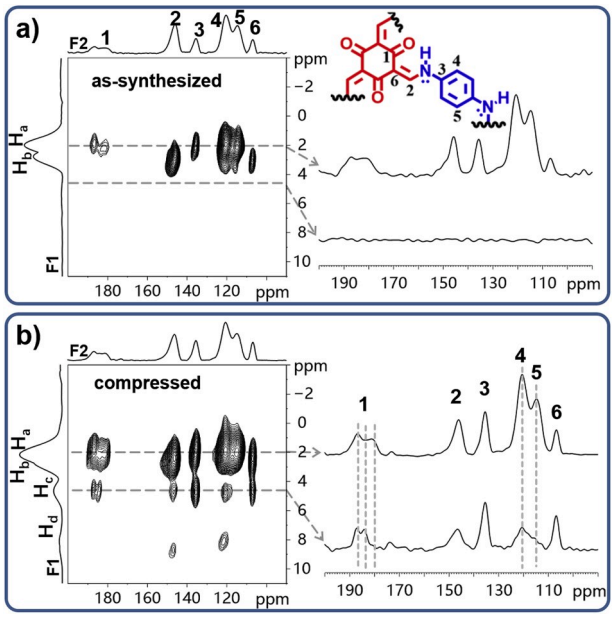


**Fig. 3.** $^{1}H$–$^{13}C$ MAS/HETCOR spectra of a) an as-synthesized TpPa-1 sample and b) a compressed TpPa-1 sample. To demonstrate the signal correlation, two 1D slice spectra were extracted from each 2D spectrum and shown in the right side of the 2D spectrum. The CP contact time in the experiments was 200 μs The $^{1}H$–$^{13}C$ MAS/HETCOR spectrum of the as-synthesized TpPa-1 acquired using a CP contact time of 100 μs can be found in Fig. S7 in Supporting Information. All experiments were conducted at 293 K.

through-space $^{1}H$–$^{13}C$ dipolar interaction.

The results given in Fig. 3a for the as-synthesized TpPa-1 sample present two $^{1}H$ resonances corresponding to the $H_a$ and $H_b$ peaks that are clearly observable along the F1 axis centered at 2.0 ppm and 2.5 ppm, respectively. In addition, seven cross peaks are observed in the 2D spectrum for this sample. The most intense cross peaks are observed at (2.0 ppm, 120.9 ppm), (2.0 ppm, 114.8 ppm), and (2.5 ppm, 146.0 ppm), which can be assigned to cross peaks between $H_a$ and C4, $H_a$ and C5, and $H_b$ and C2, respectively. However, the cross peaks between $H_a$ and C3 (2.0 ppm, 146.0 ppm), $H_b$ and C6 (2.5 ppm, 106.8 ppm), and $H_a$ and C1 (2.0 ppm, 187.5/182.0 ppm) are relatively weak because these carbon positions have no directly bonded protons, which makes the $^{1}H$–$^{13}C$ dipole coupling relatively weak. Interestingly, no cross peaks associated with water molecules are observed, as indicated by the line F1 = 4.5 ppm on the left side of Fig. 3a and its one-dimensional (1D) slice spectrum plotted on the right side. This indicates that interactions between water molecules and the chemical groups of TpPa-1 are very weak, which agrees well with the observations made with respect to the $^{1}H$ DQ-SQ correlation spectrum of this sample. Besides, in Fig. 3a no cross peak associated with the amino groups is observed, indicating that no carbon groups are in proximity to the amino groups.

It is worthy of note that, while the cross peak between $H_a$ and C1 is weak, as discussed above, the cross peak is clearly observable. The presence of this cross peak indicates that the aromatic rings are in close proximity to the carbonyl groups. However, an analysis of the chemical structure of TaPa-1 indicates that the protons of an aromatic ring are five bonds away from the corresponding carbonyl group. This conflicts with the short contact time used in the experiments, which can only correlate $^{1}H$–$^{13}C$ spin pairs with a short distance between the spins [23]. Therefore, the cross peaks are most likely not from the correlation of intramolecular $^{1}H$–$^{13}C$ spin pairs, but rather from the correlation of the intermolecular $^{1}H$–$^{13}C$ spin pairs from neighboring layers. Accordingly, we propose that the planes of the aromatic rings are most likely tilted with respect to the planes of the cyclohexane trione rings. Such a stereo geometry could lead to a sufficient spatial proximity between the protons of the aromatic rings and the carbonyl groups to provide the weak but clear $H_a$ - C1 cross peak shown in Fig. 3a. A detailed investigation of the stereo geometry of the different chemical groups in TpPa-1 is an on-going work in our laboratory.

Fig. 3b shows the 2D $^{1}H$–$^{13}C$ HETCOR spectrum of the compressed TpPa-1 sample. The remarkable difference between the spectra in Fig. 3b and a is the appearance of cross peaks between the water molecules and the chemical groups of TpPa-1. These cross peaks indicate that the water molecules interact with the chemical groups of TpPa-1 in the compressed sample. A comparison of the 1D slice spectra associated with the lines F1 = 2.0 ppm and F1 = 4.5 ppm presented on the right side of the 2D spectrum indicates that the C4 and C5 signals are not as strong along the line F1 = 4.5 ppm as those observed along the line F1 = 2.0 ppm. This suggests that the water molecules are not prone to interact with the C4 and C5 carbon atoms, which can be attributed to the hydrophobicity of the aromatic ring. It is interesting to note that the correlation peaks observed between the carbonyl group C1 signals and the $H_c$ signal of the water molecules are different than those observed between C1 and the aromatic ring $H_a$ signal. This difference suggests that the water molecules selectively interact with a proportion of the carbonyl groups in the sample. As such, this can be considered to be an indication that the water molecules are inhomogeneously distributed in the compressed TpPa-1 sample.

The NMR observations in this work have clearly demonstrated that the water molecules in the as-synthesized samples are likely present only inside the pore spaces, which is in agreement with the findings of previous studies [4,24]. A clear absence of strong interactions between the water molecules and the chemical groups of TpPa-1 has been observed, even though the COF contains hydrophilic groups such as carbonyl and amino groups. This can be attributed to the formation of strong intramolecular hydrogen bonding between the amino groups and neighboring carbonyl groups, which hinders the formation of hydrogen bonds between the water molecules and the amino/carbonyl groups. In contrast, the NMR results for the compressed samples indicate that the water molecules interact with the chemical groups of TpPa-1. This is very likely due to the relocation of the water molecules, caused by the transport of water molecules into the interstices between the TpPa-1 layers [16]. However, the nearly constant signals in the $^{1}H$ NMR spectra (Fig. 1c) and the $^{13}C$ NMR spectra (Fig. 2a) before and after compression indicate that the presence of these interstitial water molecules fails to disturb the intramolecular hydrogen bonding between the carbonyl and amino groups. Nonetheless, the clear interactions between the water molecules and the chemical groups of TpPa-1, as reflected by all of the $H_c$ - C*i* (*i* = 1–6) correlation peaks in the 2D HETCOR spectrum in Fig. 3b verify the presence of water molecules in these interstitial spaces. Note that the correlation peaks between the water signal and those of C4 and C5 are relatively weak, indicating that the water molecules are not in proximity to the aromatic rings. This can be associated with the hydrophobic property of aromatic rings. In the literatures, the formation of hydrogen bonding always causes a low-field shift of the $^{1}H$ signal [23,24]. However, in this work although the water molecules have clear interaction with the chemical groups of TpPa-1, the chemical shift of the water signal remains unchanged. This strongly indicates that there is no strong hydrogen bonding between the water molecules and the chemical groups of TpPa-1. Accordingly, the observed interaction signals can be attributed to electrostatic interactions between water molecules and hydrophilic atoms (i.e., the oxygen atoms of the carbonyl groups and the nitrogen atoms of the amino groups) [27]. As a result, the signals of the carbon atoms in proximity to the carbonyl groups (C1 and C6) and the amino groups (C2 and C3) are selectively enhanced in the extracted spectra shown in the right side of Fig. 3b. Naturally, the hydrophobicity of the aromatic rings and their relatively large spatial separation from the hydrophilic groups in the TpPa-1 structure greatly limits interactions between water molecules and aromatic rings.

The above-discussed interactions between water molecules and the chemical groups of TpPa-1 can be employed to achieve a deeper

understanding of the factors affecting the water permeance of this material. As discussed, it is known that water molecules are likely present in the pore spaces of TpPa-1. Accordingly, the water permeance of this material thus result primarily from the transport of water molecules through the pores spaces of TpPa-1. Yet, the experimental observations in this work also demonstrate that the water molecules can enter into the interstices between the layers of the compressed TpPa-1 sample. As such, this additional transport route for water molecules may decrease the water permeance of this material by increasing its interior resistance [28]. This provides a plausible explanation for why the water permeance of a single layer of TpPa-1 is always much greater than that of multi-layered TpPa-1 [29,30]. However, our results indicate that water molecules will not spontaneously enter into the interstices between the layers of TpPa-1 in the absence of compression, but that this entering process is facilitated within the compressed TpPa-1 samples. After entering the interstices, the water molecules are prone to surround the hydrophilic groups, such as the carbonyl and amino groups, but reside relatively far from the aromatic rings. This process then results in an inhomogeneous distribution of water molecules within the interstices between the TpPa-1 layers.

## 4. Conclusion

We have presented a detailed study of the locations and interactions of water molecules absorbed on the surfaces of TpPa-1 materials based on a variety of advanced solid-state NMR techniques. The TpPa-1 samples included as-synthesized powder samples and powder samples first subjected to compression at high pressure and then ground into a powder form. The results of XRD and various NMR techniques indicated that the compression process had no effect on the crystal and chemical structures of TpPa-1, but that the adsorbed water molecules in the as-synthesized and compressed TpPa-1 powder samples can exist in different locations and bonding states. The adsorbed water molecules in the as-synthesized TpPa-1 samples were found to be mainly located in the pore spaces and interacted only loosely with the chemical groups of TpPa-1. In contrast, a proportion of the water molecules in the compressed TpPa-1 samples were found to enter into the interstices between the TpPa-1 layers and interact with the amino groups and the carbonyl groups of the material. The presence of interstitial water molecules in the compressed sample was shown to provide a plausible molecular origin for the increased water adsorption capability of the material under pressure. On a molecular level, the NMR results clearly demonstrated that no strong hydrogen bonding exists between the water molecules and the chemical groups of TpPa-1 in either the as-synthesized samples or the compressed samples. However, the water molecules in the interstices between the layers of the compressed sample were shown to be preferentially located in proximity to the carbonyl groups and the nitrogen atoms of the amino groups. The origin of the interactions between water molecules and the chemical groups of TpPa-1 was attributed to electrostatic interactions between water molecules and the hydrophilic atoms in the material (i.e., the oxygen atoms of the carbonyl groups and the nitrogen atoms of the amino groups). This interaction can be expected to facilitate the transport of water molecules in the material, and therefore provides a plausible molecular origin for the high permeance of this material.

## CRediT authorship contribution statement

**Jiaqi Ma:** Investigation, Data curation, Formal analysis, Writing - original draft, Writing - review & editing. **Xiao-Bin Fu:** Investigation, Data curation, Formal analysis. **Yuquan Li:** Investigation, Data curation. **Tian Xia:** Investigation, Data curation, Formal analysis. **Likun Pan:** Writing - review & editing. **Ye-Feng Yao:** Conceptualization, Methodology, Writing - original draft, Supervision, Formal analysis, Writing - review & editing.

## Acknowledgments

This work was supported by the National Key Research and Development Program of China (Grant No. 2018YFC1602800, 2018YFF01012504), National Natural Science Foundation of China (Grant No. 21574039) and Microscale Magnetic Resonance Platform of ECNU.

## Appendix A. Supplementary data

Supplementary data to this article can be found online at https://doi.org/10.1016/j.micromeso.2020.110287.

## References

[1] A.P. Côté, A.I. Benin, N.W. Ockwig, M. O'Keeffe, A.J. Matzger, O.M. Yaghi, Porous, crystalline, covalent organic frameworks, Science 310 (2005) 1166–1170, https://doi.org/10.1126/science.1120411.
[2] W. Zhang, L. Zhang, H. Zhao, B. Li, H. Ma, A two-dimensional cationic covalent organic framework membrane for selective molecular sieving, J. Mater. Chem. A. 6 (2018) 13331–13339, https://doi.org/10.1039/c8ta04178d.
[3] X. Zhang, H. Li, J. Wang, D. Peng, J. Liu, Y. Zhang, In-situ grown covalent organic framework nanosheets on graphene for membrane-based dye/salt separation, J. Membr. Sci. 581 (2019) 321–330, https://doi.org/10.1016/j.memsci.2019.03.070.
[4] W. Zhou, M. Wei, X. Zhang, F. Xu, Y. Wang, Fast desalination by multilayered covalent organic framework (COF) nanosheets, ACS Appl. Mater. Interfaces 11 (2019) 16847–16854, https://doi.org/10.1021/acsami.9b01883.
[5] G. Li, J. Ye, Q. Fang, F. Liu, Amide-based covalent organic frameworks materials for efficient and recyclable removal of heavy metal lead (II), Chem. Eng. J. 370 (2019) 822–830, https://doi.org/10.1016/j.cej.2019.03.260.
[6] M. Zhang, R. Zheng, Y. Ma, R. Chen, X. Sun, X. Sun, N-rich covalent organic frameworks with different pore size for high-pressure CO2 adsorption, Microporous Mesoporous Mater. 285 (2019) 70–79, https://doi.org/10.1016/j.micromeso.2019.04.021.
[7] S. Li, Y. Yang, H. Shan, J. Zhao, Z. Wang, D. Cai, P. Qin, J. Baeyens, T. Tan, Ultrafast and ultrahigh adsorption of furfural from aqueous solution via covalent organic framework-300, Separ. Purif. Technol. 220 (2019) 283–292, https://doi.org/10.1016/j.seppur.2019.03.072.
[8] X. Shi, Y. Yao, Y. Xu, K. Liu, G. Zhu, L. Chi, G. Lu, Imparting catalytic activity to a covalent organic framework material by nanoparticle encapsulation, ACS Appl. Mater. Interfaces 9 (2017) 7481–7488, https://doi.org/10.1021/acsami.6b16267.
[9] M. Matsumoto, L. Valentino, G.M. Stiehl, H.B. Balch, A.R. Corcos, F. Wang, D. C. Ralph, B.J. Marinas, W.R. Dichtel, Lewis-acid-catalyzed interfacial polymerization of covalent organic framework films, Inside Chem. 4 (2018) 308–317, https://doi.org/10.1016/j.chempr.2017.12.011.
[10] Y. Yang, X.-J. Hong, C.-L. Song, G.-H. Li, Y.-X. Zheng, D.-D. Zhou, M. Zhang, Y.-P. Cai, H. Wang, Lithium bis(trifluoromethanesulfonyl)imide assisted dual-functional separator coating materials based on covalent organic frameworks for high-performance lithium–selenium sulfide batteries, J. Mater. Chem. A. 7 (2019) 16323–16329, https://doi.org/10.1039/C9TA04614C.
[11] Q. Sun, B. Aguila, J. Perman, L.D. Earl, C.W. Abney, Y. Cheng, H. Wei, N. Nguyen, L. Wojtas, S. Ma, Postsynthetically modified covalent organic frameworks for efficient and effective mercury removal, J. Am. Chem. Soc. 139 (2017) 2786–2793, https://doi.org/10.1021/jacs.6b12885.
[12] L. Tang, H. Chen, J. Song, Process of pore pressure diffusion in saturated clay soil and impact of adsorbed water, Geosci. J. 20 (2016) 649–665, https://doi.org/10.1007/s12303-016-0002-4.
[13] B. Assfour, G. Seifert, Adsorption of hydrogen in covalent organic frameworks: comparison of simulations and experiments, Microporous Mesoporous Mater. 133 (2010) 59–65, https://doi.org/10.1016/j.micromeso.2010.04.015.
[14] S. Wang, Z. Zhang, H. Zhang, A.G. Rajan, N. Xu, Y. Yang, Y. Zeng, P. Liu, X. Zhang, Q. Mao, Y. He, J. Zhao, B.-G. Li, M.S. Strano, W.-J. Wang, Reversible polycondensation-termination growth of covalent-organic-framework spheres, fibers, and films, Matter (2019), https://doi.org/10.1016/j.matt.2019.08.019.
[15] S. Jhulki, A.M. Evans, X.-L. Hao, M.W. Cooper, C.H. Feriante, J. Leisen, H. Li, D. Lam, M.C. Hersam, S. Barlow, J.-L. Brédas, W.R. Dichtel, S.R. Marder, Humidity sensing through reversible isomerization of a covalent organic framework, J. Am. Chem. Soc. (2020), https://doi.org/10.1021/jacs.9b08628.
[16] S. Kandambeth, A. Mallick, B. Lukose, M.V. Mane, T. Heine, R. Banerjee, Construction of crystalline 2D covalent organic frameworks with remarkable chemical (Acid/Base) stability via a combined reversible and irreversible route, J. Am. Chem. Soc. 134 (2012) 19524–19527, https://doi.org/10.1021/ja308278w.
[17] C.R. DeBlase, K.E. Silberstein, T.-T. Truong, H.D. Abruña, W.R. Dichtel, β-Ketoenamine-Linked covalent organic frameworks capable of pseudocapacitive energy storage, J. Am. Chem. Soc. 135 (2013) 16821–16824, https://doi.org/10.1021/ja409421d.
[18] B.P. Biswal, S. Kandambeth, S. Chandra, D.B. Shinde, S. Bera, S. Karak, B. Garai, U. K. Kharul, R. Banerjee, Pore surface engineering in porous, chemically stable covalent organic frameworks for water adsorption, J. Mater. Chem. 3 (2015) 23664–23669, https://doi.org/10.1039/c5ta07998e.

[19] S.P. Brown, I. Schnell, J.D. Brand, K. Müllen, H.W. Spiess, An investigation of π−π packing in a columnar hexabenzocoronene by fast magic-angle spinning and double-quantum 1H solid-state NMR spectroscopy, J. Am. Chem. Soc. 121 (1999) 6712–6718, https://doi.org/10.1021/ja990637m.
[20] M. Feike, D.E. Demco, R. Graf, J. Gottwald, S. Hafner, H.W. Spiess, Broadband multiple-quantum NMR spectroscopy, J. Magn. Reson., Ser. A 122 (1996) 214–221, https://doi.org/10.1006/jmra.1996.0197.
[21] H. Shigenobu, H. Kikuko, Chemical shift standards in high-resolution solid-state NMR (1) 13C, 29Si, and 1H nuclei, Bull. Chem. Soc. Jpn. 64 (1991) 685–687, https://doi.org/10.1246/bcsj.64.685.
[22] M. Sigalov, B. Shainyan, N. Chipanina, I. Ushakov, A. Shulunova, Intra- and intermolecular N-H···O hydrogen bonds in pyrrolyl derivatives of indane-1,3-dione – experimental and theoretical study, J. Phys. Org. Chem. 22 (2009) 1178–1187, https://doi.org/10.1002/poc.1573.
[23] H.-H. Limbach, P.M. Tolstoy, N. Pérez-Hernández, J. Guo, I.G. Shenderovich, G. S. Denisov, OHO hydrogen bond geometries and NMR chemical shifts: from equilibrium structures to geometric H/D isotope effects, with applications for water, protonated water, and compressed ice, Isr. J. Chem. 49 (2009) 199–216, https://doi.org/10.1560/IJC.49.2.199.
[24] J. Emsley, Very strong hydrogen bonding, Chem. Soc. Rev. 9 (1980) 91–124, https://doi.org/10.1039/CS9800900091.
[25] L. Kobera, S.A. Southern, J.M. Frost, D.L. Bryce, Multinuclear solid-state magnetic resonance study of oxo-bridged diniobium and quadruply-bonded dimolybdenum carboxylate clusters, Solid State Nucl. Magn. Reson. 84 (2017) 20–27, https://doi.org/10.1016/j.ssnmr.2016.12.001.
[26] M. Polissiou, M.T.P. Viet, M. St-Jacques, T. Theophanides, Binding study of the drug cis-dichlorodiammineplatinum (II) to G p5' and dGp5' by high resolution proton and carbon-13 NMR spectroscopy, Inorg. Chim. Acta. 107 (1985) 203–210, https://doi.org/10.1016/S0020-1693(00)80704-5.
[27] Z. Gu, C.F. Ridenour, C.E. Bronnimann, T. Iwashita, A. McDermott, Hydrogen bonding and distance studies of amino acids and peptides using solid state 2D 1H−13C heteronuclear correlation spectra, J. Am. Chem. Soc. 118 (1996) 822–829, https://doi.org/10.1021/ja952130r.
[28] J. Pérez-Carvajal, G. Boix, I. Imaz, D. Maspoch, The imine-based COF TpPa-1 as an efficient cooling adsorbent that can Be regenerated by heat or light, Adv. Energy Mater. 9 (2019), https://doi.org/10.1002/aenm.201901535, 1901535.
[29] K. Higashi, K. Yamamoto, M.K. Pandey, K.H. Mroue, K. Moribe, K. Yamamoto, A. Ramamoorthy, Insights into atomic-level interaction between mefenamic acid and eudragit EPO in a supersaturated solution by high-resolution magic-angle spinning NMR spectroscopy, Mol. Pharm. 11 (2014) 351–357, https://doi.org/10.1021/mp4005723.
[30] A. Xiao, Z. Zhang, X. Shi, Y. Wang, Enabling covalent organic framework nanofilms for molecular separation: perforated polymer-assisted transfer, ACS Appl. Mater. Interfaces 11 (2019) 44783–44791, https://doi.org/10.1021/acsami.9b18062.